

Supplementary Information

Dynamic Coordination of Cations and Catalytic Selectivity on Zn-Cr Oxide Alloy during Syngas Conversion

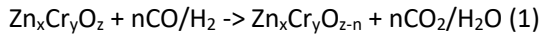
Sicong Ma, Si-da Huang and Zhi-Pan Liu*

Corresponding Author: *zpliu@fudan.edu.cn

Collaborative Innovation Centre of Chemistry for Energy Material, Shanghai Key Laboratory of Molecular Catalysis and Innovative Materials, Key Laboratory of Computational Physical Science, Department of Chemistry, Fudan University, Shanghai 200433, China

Supplementary Methods

Ab-initio thermodynamics analyses. To determine the equilibrium O_v concentration in ZnCrO bulk and surfaces, the *ab-initio* thermodynamics analyses have been performed where the formula



are used to compute the free energy change as a function of temperature and CO/H₂ partial pressure.

To determine the Gibbs free energy change (ΔG) per formula unit (f.u.) for the above reactions, one needs to compute

$$\begin{aligned} \Delta G(p, T) = & G[\text{ZnCrO}_x](p, T) + (y - x) * \mu[\text{H}_2\text{O}](p, T) - \\ & G[\text{ZnCrO}_y](p, T) - (y - x) * \mu[\text{H}_2](p, T) \end{aligned} \quad (2)$$

Or

$$\begin{aligned} \Delta G(p, T) = & G[\text{ZnCrO}_x](p, T) + (y - x) * \mu[\text{CO}_2](p, T) - \\ & G[\text{ZnCrO}_y](p, T) - (y - x) * \mu[\text{CO}](p, T) \end{aligned} \quad (3)$$

where G is the Gibbs free energy of bulks/surfaces and μ is the chemical potential for molecules. The $G[X]$ can be approximated by their DFT total energy $E[X]$ with appropriate inclusion of zero-point-energy (**ZPE**), since it is known that the vibration entropy and the **pV** term contributions of solid phases are negligibly small. The chemical potential for molecules $\mu[X]$ can be calculated as follows:

$$\begin{aligned} \mu[X](p, T) = & E[X] + \text{ZPE}[X] + \\ & [H[X](p^0, T) - H[X](p^0, 0K) - TS[X](p^0, T) + k_B T \ln \frac{p}{p^0}] \end{aligned}$$

where enthalpy (**H**) and entropy (**S**) terms are taken from the standard thermodynamics data.

Computation for methanol yield. Our calculated methanol generation rate are $\sim 250 \text{ s}^{-1}$ at 573 K and 2.5 MPa syngas (H₂:CO = 1.5) on Zn₃Cr₃O₈ crystal. To estimate the methanol yield in g/(kg_{cat}*h) to compare with experiment, we make the following derivation.

On Zn₃Cr₃O₈ (0001) surface, each active site occupies the surface area of 30.572 Å².

Assumption 1: the real Zn₃Cr₃O₈ catalyst nanoparticle is assumed to follow the thermodynamic Wulff morphology (Supplementary Figure 3) with the specific surface area of $\sim 100 \text{ m}^2/\text{g}$.¹ It indicates that the specific surface area of (0001) surface is 44 m²/g.

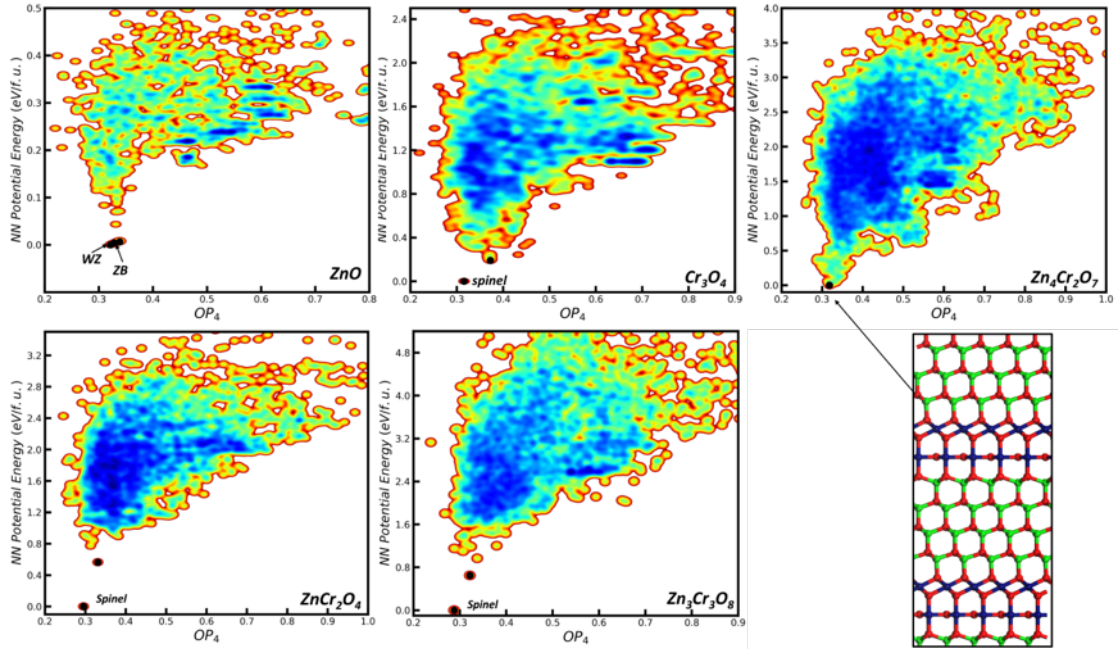
Assumption 2: the effective active sites are assumed no more than 10 %.

The total number of active sites for Zn₃Cr₃O₈ catalyst is

$$0.1 * 44 * 10^{20} * 1000 / 30.572 \text{ kg}_{\text{cat}}^{-1} = 1.439 * 10^{22} \text{ kg}_{\text{cat}}^{-1}$$

The CH₃OH generation rate is

$$250 \text{ s}^{-1} = 3600 * 250 * 1.439 * 10^{22} / (6.02 * 10^{23}) / 32 \text{ g}/(\text{kg} * \text{h}) = 672 \text{ g}/(\text{kg} * \text{h})$$



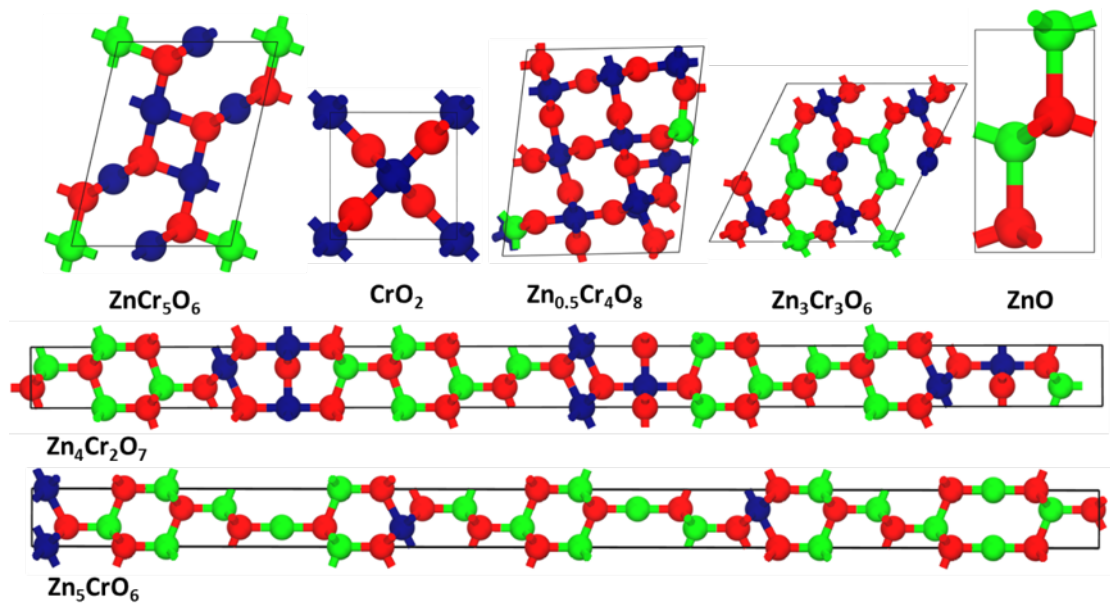
Supplementary Figure 1 | Global PESs of ZnO , Cr_3O_4 , $\text{Zn}_4\text{Cr}_2\text{O}_7$, ZnCr_2O_4 and $\text{Zn}_3\text{Cr}_3\text{O}_8$ as determined from SSW-NN global search. Each plot contains more than 10,000 minima. The energy (eV/f.u.) of most stable phase is set as reference zero. The x axis is the common structure fingerprint for the crystal, namely, the distance-weighted Steinhardt-type order parameter (OP) with angular moment $L = 4$ which can distinguish different minima (the definition of OP is described in our previous paper), and the y axis is the relative energy (ΔE) of minima.

For the ZnO , the identified most stable structure is wurtzite (WZ) phase, which is the commonly observed phase under ambient pressure, followed by zinc blende phase (ZB) which is 4 meV/f.u. less stable than WZ phase.² For Cr_3O_4 , ZnCr_2O_4 and $\text{Zn}_3\text{Cr}_3\text{O}_8$ phase, the global minimum adopts the spinel-type skeleton. The $\text{Zn}_4\text{Cr}_2\text{O}_7$ phase can be regarded as a mixture of ZnO (WZ) and Cr_2O_3 phase.

Supplementary Table 1 | Geometric parameters of ZnCrO compositions.

Properties	Group name	Number	a, b, c (Å)	α , β, γ(°)	CN (Cr) ^a	CN (Zn)
ZnCr ₂ O ₄	Fd-3m	#227	8.386, 8.386, 8.386	90, 90, 90	6	4
Zn ₃ Cr ₃ O ₈	R-3m	#166	5.942, 5.942, 14.504	90, 90, 120	6	4, 6
Zn _{1.5} Cr ₄ O ₈	Cmcm	#63	11.857, 16.759, 5.909	90, 90, 90	6	4
Zn ₅ Cr ₁ O ₆	R3m	#160	3.161, 3.161, 50.071	90, 90, 120	6	2, 4
Zn ₄ Cr ₂ O ₆	P-4m2	#115	3.136, 3.136, 14.913	90, 90, 90	4	4
Zn ₃ Cr ₃ O ₆	C2/m	#12	10.082, 2.995, 9.841	90, 116, 90	4, 6	4, 6
Zn ₂ Cr ₄ O ₆	C2/m	#12	10.223, 3.008, 9.864	90, 63, 90	4, 6	4
ZnCr ₅ O ₆	P2	#3	8.056, 3.039, 6.137	90, 102, 90	4	4
CrO	P4 ₂ /mmc	#131	3.047, 3.047, 5.401	90, 90, 90	4	--
Cr ₃ O ₄	I4 ₁ /amd	#141	6.262, 6.262, 7.607	90, 90, 90	4, 6	--
Cr ₂ O ₃	R-3	#148	5.095, 5.095, 14.141	90, 90, 120	6	--
CrO ₂	P4 ₂ /mnm	#136	4.437, 4.437, 2.948	90, 90, 90	6	--

^a coordination number



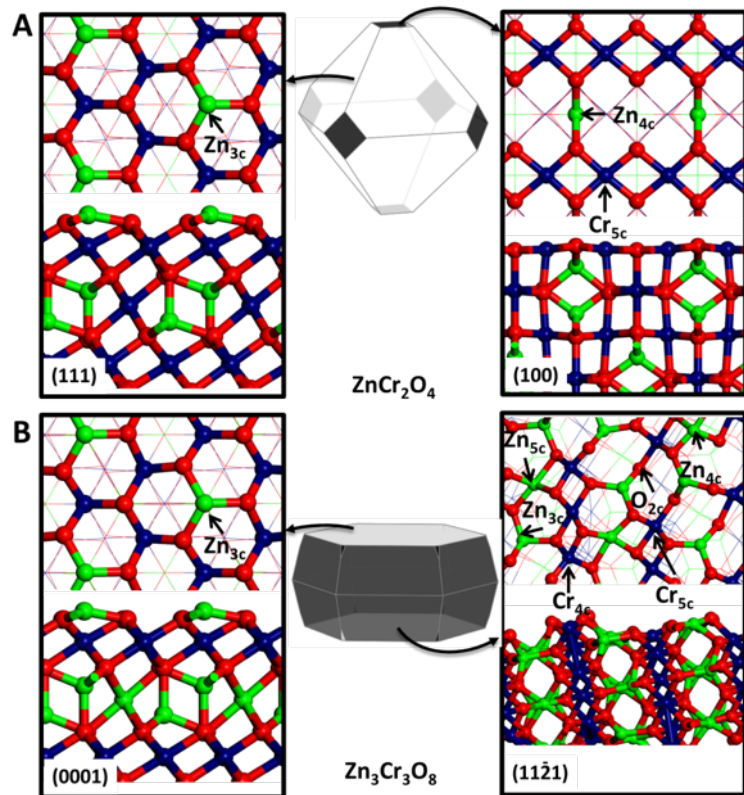
Supplementary Figure 2 | The most stable structures for different ZnCrO compositions.

Supplementary Table 2 | Surface energies and surface compositions of ZnCr₂O₄ and Zn₃Cr₃O₈.*

Surface	γ (J/m ²)	Surface composition
ZnCr ₂ O ₄ (100)	1.04	Zn _{4c} , Cr _{5c} , O _{3c}
ZnCr ₂ O ₄ (110)	1.65	Cr _{4c} , O _{2c} , O _{3c}
ZnCr ₂ O ₄ (111)	0.75	Zn _{3c} , O _{3c}
Zn ₃ Cr ₃ O ₈ (0001)	0.66	Zn _{3c} , O _{3c}
Zn ₃ Cr ₃ O ₈ (1121)	1.23	Zn _{3c} , Cr _{4c} , Cr _{5c} , O _{2c} , O _{3c}
Zn ₃ Cr ₃ O ₈ (1120)	1.28	Zn _{3c} , Zn _{4c} , Cr _{4c} , O _{3c}
Zn ₃ Cr ₃ O ₈ (1011)	1.42	Zn _{3c} , Cr _{5c} , O _{2c}

*The surface energy is calculated at 0 K.

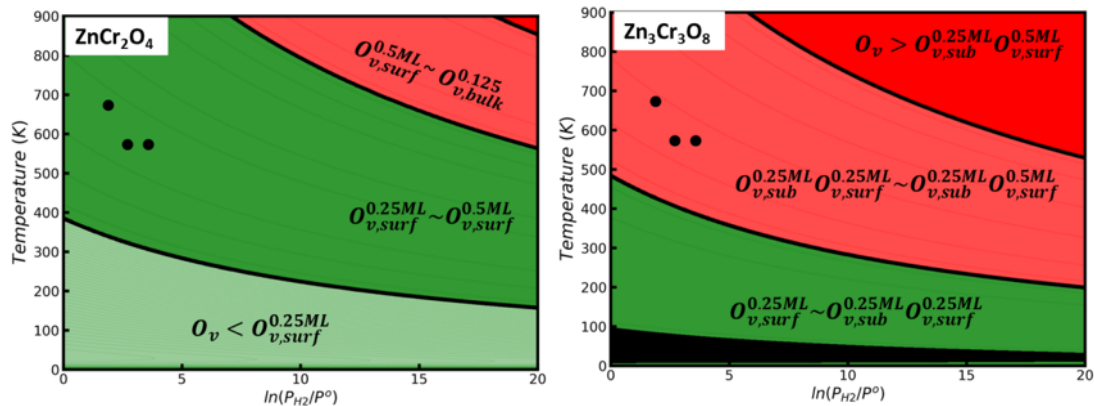
Typically, the surface energies (γ) of low miller index surface can be calculated via a symmetrical slab using $\gamma = (E_{slab} - nE_{bulk})/2A$, where E_{slab} denotes the slab energy and nE_{bulk} is the energy of the n units in the bulk model which sums up to have the same atom number with slab model. γ is normalized to energy per unit area by dividing through the total surface area 2A. However, for the ZnCr₂O₄ and Zn₃Cr₃O₈ facets with varied terminations, it is unlikely to cut out a symmetric slab and keep the chemical stoichiometry (ZnCr₂O₄ or Zn₃Cr₃O₈). Therefore, we have added extra Zn, Cr or O atoms in the slab to construct a symmetric slab and fast searched for the best surface configurations. The stable candidates are computed using DFT, where the surface energy are calculated via the $\gamma = (E_{slab-Zn_xCr_yO_z} - x\mu_{ZnO} - y\mu_{Cr} - \frac{z-x}{2}\mu_{O_2})/2A$, where μ_{Cr} is determined from $\mu_{ZnCr_2O_4} = \mu_{ZnO} + 2\mu_{Cr} + 3/2\mu_{O_2}$ or $\mu_{Zn_3Cr_3O_8} = 3\mu_{ZnO} + 3\mu_{Cr} + 5/2\mu_{O_2}$. The surface energy is therefore finally referring to $\mu_{ZnCr_2O_4}$, $\mu_{Zn_3Cr_3O_8}$, μ_{ZnO} and μ_{O_2} .



Supplementary Figure 3 | The exposed surface structures and predicted Wulff morphologies for ZnCr_2O_4 and $\text{Zn}_3\text{Cr}_3\text{O}_8$.

The identified most stable facets for ZnCr_2O_4 is the (111) facet, followed by the (100) and (110) facets. According to the Wulff construction relationship and the computed surface energies, the predicted morphology of ZnCr_2O_4 at 0 K is a truncated octahedron exposing majority (111) facet (92.7 %) and minority (100) facet (7.3 %).

The identified most stable facets for $\text{Zn}_3\text{Cr}_3\text{O}_8$ is the (0001) facet, followed by the (1121), (1120) and (1011) facets. Similarly, the predicted Wulff equilibrium morphology of $\text{Zn}_3\text{Cr}_3\text{O}_8$ is a truncated dodecahedron with the 44.0 % (0001)-A facet, 55.6 % (1121) facet and 0.4 % (1011) facet.



Supplementary Figure 4 | Thermodynamic phase diagram of O_v concentration for $ZnCrO$ catalysts in contact with H_2 . The phase diagram is computed from the free energy data based on DFT energetics. The pressures of reduced products H_2O is assumed as 0.1 kPa.

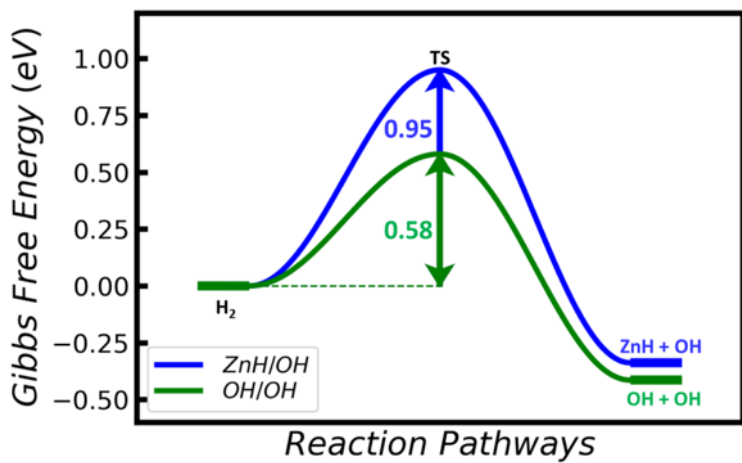
Supplementary Table 3 | The oxygen vacancy (O_v) formation energy on the most stable surfaces of $ZnCrO$ referring to the gas O_2 at 0 K.

O_v type (concentration)	E_{Ov} (eV, $ZnCr_2O_4$)	E_{Ov} (eV, $Zn_3Cr_3O_8$)
$O_{v,bulk}^{0.125}$	4.71	3.10
$O_{v,surf}^{0.25ML}$	2.66	2.21
$O_{v,surf}^{0.5ML}$	3.85	3.54
$O_{v,sub}^{0.25ML} O_{v,surf}^{0.25ML}$	3.90	2.78

Supplementary Table 4 | The adsorption energies (E_{ads} , eV) of CO and H₂ on different facets.

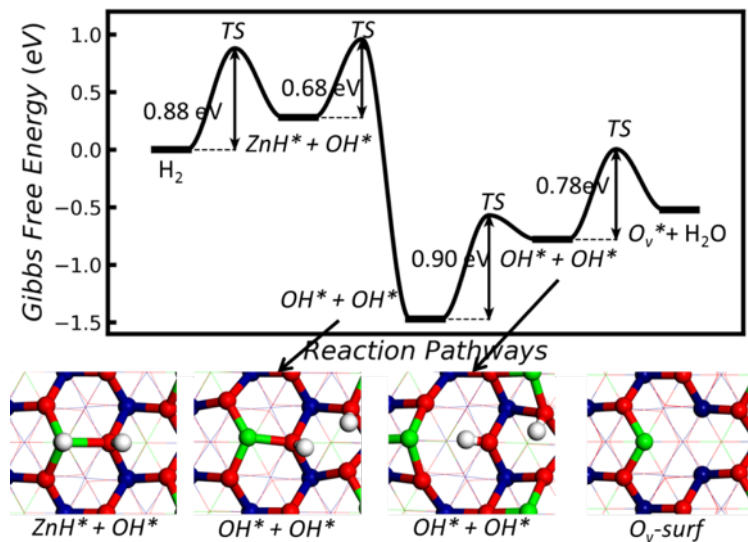
Surface	$E_{ads,CO}$	E_{ads,H_2}
Perfect ZnCr ₂ O ₄ (111)	-0.39	-2.47
Perfect Zn ₃ Cr ₃ O ₈ (0001)	-0.4	-3.02
ZnCr ₂ O ₄ $O_{v,surf}^{0.25ML}$ – 111	-0.54	-1.38
Zn ₃ Cr ₃ O ₈ $O_{v,surf}^{0.25ML} O_{v,sub}^{0.25ML}$ – 0001	-0.44	-1.48

The CO and H₂ adsorption properties are examined, see Supplementary Table 4. For the perfect (111)-A and (0001)-A surfaces with the exposure of Zn_{3c} and O_{3c} atoms, CO molecule can be adsorbed on the Zn_{3c} sites with the Zn-C bond length of 2.12 Å, being slightly exothermic by 0.40 eV. Hydrogen molecule can dissociatively adsorb on O_{3c} sites with a large energy release (> 2.4 eV). However, for the O-vacant surfaces with the exposure of Cr and Zn atoms, CO molecule still tends to be coordinated with Zn atom with the shortened Zn-C bond of 2.05 Å and slightly strengthened adsorption energy ($E_{ads} = \sim -0.5$ eV). The calculated CO adsorption properties are consistent with the experimental calorimetric isotherms results that the adsorption heat is between 50 and 80 kJ/mol (corresponding to 0.5 ~ 0.8 eV).³ Instead, the existence of O_v dramatically weakens H₂ dissociative adsorption ($E_{ads} = \sim -1.4$ eV).



Supplementary Figure 5 | The H₂ dissociation on Zn₃Cr₃O₈ O_{v,surf}^{0.25ML} O_{v,sub}^{0.25ML}(0001) surface.

For the O-defective Zn₃Cr₃O₈ surface, the lowest energy pathway for H₂ dissociation prefers the O-O pair mechanism, as shown in Supplementary Figure 5.

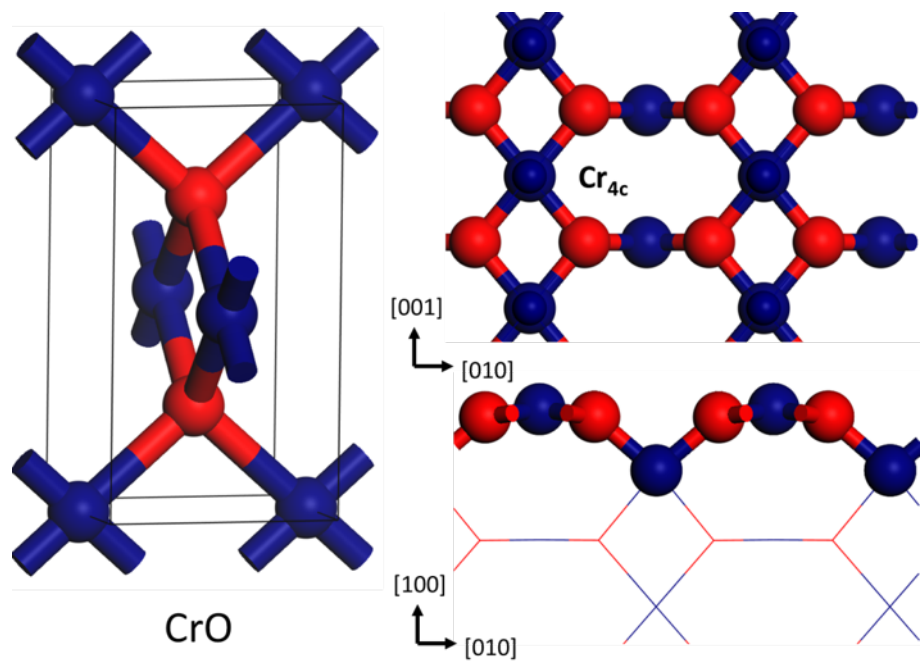


Supplementary Figure 6 | The H₂-assisted O_v formation process on ZnCr₂O₄ (111) surface.

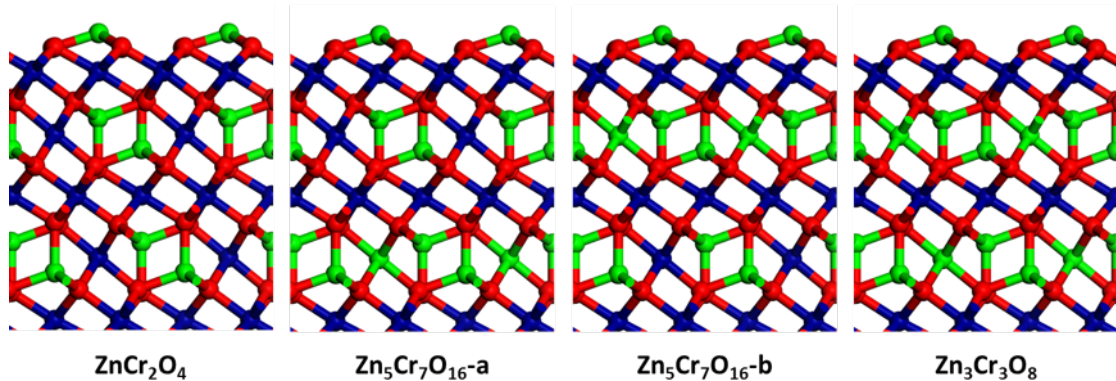
Supplementary Figure 6 shows the calculated free energy profile ($T = 573\text{ K}$, $P_{\text{H}_2} = 1.5\text{ MPa}$) for the surface O removal to generate O_v assisted by H₂ reactant. The overall reaction barrier for the O_v generation is 1.47 eV, lower than 1.75 eV for methane production on ZnCr₂O₄ and thus does not affect the reaction activity and selectivity. As shown, the H₂ dissociates to the surface Zn_{3c} and O_{3c} atoms with the reaction barrier of 0.88 eV. Then, the H on Zn atom migrates to the surface O atom with the barrier of 0.68 eV and the reaction free energy of -1.75 eV. Then the combination of two OH groups, involving a series of structural change with the cleavage of Zn-O and Cr-O bonds, needs to overcome 1.47 eV barriers to yield O_v and H₂O molecule.

Supplementary Table 5 | The syngas conversion reaction energy barrier and reaction rate constant at 573 K and 2.5 MPa syngas.

Zn ₃ Cr ₃ O ₈ O _{v,surf} ^{0.25ML} O _{v,sub} ^{0.25ML} – 0001	E _{a,+}	E _{a,-}	k ₊	k ₋
CO + * -> CO*	0.984	0.441	2.64E+04	1.57E+09
H ₂ + 2** -> 2H**	0.585	0.809	8.61E+07	9.17E+05
CO* + H** -> CHO* + **	0.275	0.248	4.57E+10	7.90E+10
CHO* + H** -> CH ₂ O* + **	0.845	0.491	4.28E+05	5.78E+08
0.5H ₂ + ** -> H**	0.292	0.851	3.21E+10	3.87E+05
CH ₂ O* + H** -> CH ₃ O* + **	0.504	1.064	4.37E+08	5.19E+03
H ₂ + 2** -> 2H**	0.585	0.628	8.61E+07	3.58E+07
CH ₃ O* + H** -> CH ₃ OH + * + **	1.328	--	2.51E+01	0.00E+00
CH ₃ O* + H** -> CH ₄ + O* + **	2.407	--	8.01E-09	0.00E+00
Zn ₃ Cr ₃ O ₈ O _{v,surf} ^{0.25ML} – 111	E _{a,+}	E _{a,-}	k ₊	k ₋
CO + * -> CO*,	0.984	0.543	2.64e+04	1.98e+08
H ₂ + 2** -> 2H**, ,	0.585	0.698	8.61e+07	8.66e+06
CO* + H** -> CHO* + **	0.307	0.261	2.39e+10	5.98e+10
CHO* + H** -> CH ₂ O* + **	0.765	1.008	2.22e+06	1.61e+04
0.5H ₂ + ** -> H**	0.292	1.059	3.20e+10	5.83e+03
CH ₂ O* + H** -> CH ₃ O* + **	0.668	1.158	1.58e+07	7.86e+02
0.5H ₂ + ** -> H**	0.292	0.679	3.20e+10	1.26e+07
CH ₃ O* + H** -> CH ₃ OH + * + **	2.504	--	1.13e-09	--
CH ₃ O* + H** -> CH ₄ + O* + **	1.747	--	5.16e-03	--



Supplementary Figure 7 | The structures of CrO crystal ($P42/mmc$, #131) and (100) surface with the exposure of planar $[CrO_4]$ and O_{3c} atoms.



Supplementary Figure 8 | The surface models for ZnCr_2O_4 , $\text{Zn}_5\text{Cr}_7\text{O}_{16}$ and $\text{Zn}_3\text{Cr}_3\text{O}_8$.

Supplementary Table 6 | The O_v formation energy (E_f , eV) referring to the gas O_2 at 0 K.

O_v concentration	$E_f(\text{ZnCr}_2\text{O}_4)$	$E_f(\text{Zn}_5\text{Cr}_7\text{O}_{16}\text{-a})$	$E_f(\text{Zn}_5\text{Cr}_7\text{O}_{16}\text{-b})$	$E_f(\text{Zn}_3\text{Cr}_3\text{O}_8)$
$O_{v,surf}^{0.25ML}$	2.66	2.54	2.24	2.21
$O_{v,sub}^{0.25ML} O_{v,surf}^{0.25ML}$	3.90	3.67	2.79	2.78

There are two possible structures for the most stable $\text{Zn}_5\text{Cr}_7\text{O}_{16}$ surface, distinguished by the position of $[\text{ZnO}_6]$: with or without the presence of $[\text{ZnO}_6]$ in the subsurface layer (Supplementary Figure 8). We have calculated O_v formation energies (E_f) for these two surfaces and the results are listed in Supplementary Table 6. As shown, with the presence of $[\text{ZnO}_6]$ in the subsurface, the E_f is close to that in $\text{Zn}_3\text{Cr}_3\text{O}_8$; while with the $[\text{ZnO}_6]$ in the bulk (i.e. no $[\text{ZnO}_6]$ in the subsurface), the E_f is close to that in ZnCr_2O_4 . This again confirms the importance of subsurface $[\text{ZnO}_6]$ in the formation of the subsurface O_v , which has the largest concentration when the Zn:Cr ratio reaches to 1:1.

Supplementary Table 7 | Structure information in the first principles global dataset. Listed data are the number of the structures in the global dataset, as distinguished by the chemical formula, the number of atoms per cell (N_{atom}), the type of structures (cluster, bulk and layer).

Species	N_{atom}	cluster	layer	bulk	total
O2-Zn17	19	0	7	183	190
O4-Zn15	19	0	0	21	21
O6-Zn6	12	1119	0	0	1119
O6-Zn8	14	0	15	218	233
O6-Cr1-Zn5	12	0	8	52	60
O6-Cr2-Zn4	12	0	6	183	189
O6-Cr3-Zn3	12	0	11	259	270
O6-Cr4	10	0	11	298	309
O6-Cr4-Zn2	12	196	116	2249	2561
O6-Cr5-Zn1	12	0	0	58	58
O7-Zn8	15	0	18	218	236
O7-Zn16	23	0	0	25	25
O7-Cr1-Zn5	13	0	9	68	77
O7-Cr2-Zn4	13	0	3	55	58
O7-Cr4-Zn2	13	265	262	6705	7232
O7-Cr5-Zn1	13	0	6	280	286
O7-Cr6	13	0	29	245	274
O8-Zn8	16	291	12	3851	4154
O8-Cr1-Zn5	14	0	31	485	516
O8-Cr2-Zn4	14	0	28	81	109
O8-Cr3-Zn2	13	0	11	343	354
O8-Cr3-Zn3	14	0	91	78	169
O8-Cr4	12	0	34	146	180
O8-Cr4-Zn1	13	0	7	38	45
O8-Cr4-Zn2	14	366	1359	6879	8604
O8-Cr4-Zn3	15	0	0	37	37
O8-Cr5-Zn1	14	227	8	2149	2384
O8-Cr6	14	346	6	2052	2404
O10-Zn10	20	0	1097	82	1179
O10-Zn16	26	0	1	55	56
O10-Zn24	34	0	12	249	261
O11-Zn15	26	0	0	22	22
O11-Zn16	27	0	26	0	26
O12-Cr4-Zn8	24	0	0	101	101
O12-Cr6-Zn6	24	0	5	85	90
O12-Cr8	20	0	12	117	129
O13-Zn15	28	0	134	40	174
O14-Zn15	29	0	0	39	39
O14-Zn16	30	0	144	39	183
O14-Cr6-Zn6	26	0	3	28	31

O14-Cr7-Zn4	25	0	1	15	16
O14-Cr8-Zn4	26	0	6	55	61
O14-Cr10-Zn2	26	0	1	80	81
O14-Cr12	26	0	0	47	47
O15-Cr6-Zn5	26	0	1	17	18
O16-Zn14	30	0	288	10	298
O16-Zn16	32	0	312	108	420
O16-Cr2-Zn10	28	0	0	139	139
O16-Cr3-Zn9	28	0	2	8	10
O16-Cr5-Zn6	27	0	1	3	4
O16-Cr5-Zn7	28	0	1	23	24
O16-Cr6-Zn4	26	0	0	219	219
O16-Cr6-Zn6	28	0	2	21	23
O16-Cr8	24	0	4	51	55
O16-Cr8-Zn4	28	0	0	51	51
O16-Cr9-Zn3	28	0	0	14	14
O16-Cr12	28	0	3	129	132
O18-Cr6-Zn6	30	0	0	137	137
O18-Cr8-Zn4	30	0	6	36	42
O18-Cr10-Zn2	30	0	8	54	62
O19-Cr8-Zn5	32	0	6	88	94
O21-Cr9-Zn8	38	0	56	0	56
O22-Cr8-Zn6	36	0	11	0	11
O22-Cr9-Zn5	36	0	69	4	73
O22-Cr9-Zn6	37	0	138	85	223
O22-Cr9-Zn7	38	0	227	8	235
O22-Cr9-Zn8	39	0	132	0	132
O23-Cr9-Zn8	40	0	48	0	48
O23-Cr9-Zn9	41	0	113	2	115
O23-Cr10-Zn7	40	0	31	0	31
O23-Cr11-Zn6	40	0	40	0	40
O24-Cr9-Zn8	41	0	47	0	47
O24-Cr9-Zn9	42	0	125	0	125
O24-Cr10-Zn7	41	0	44	0	44
O24-Cr11-Zn6	41	0	37	0	37
O31-Cr16-Zn8	55	0	87	1	88
O32-Cr16	48	0	12	2	14
O32-Cr16-Zn1	49	0	20	212	232
O32-Cr16-Zn2	50	0	0	15	15
O32-Cr16-Zn3	51	0	0	18	18
O32-Cr16-Zn4	52	0	9	3	12
O32-Cr16-Zn5	53	0	4	22	26
O32-Cr16-Zn8	56	0	104	2	106
O39-Cr15-Zn15	69	0	40	0	40

O40-Cr15-Zn15	70	0	53	0	53
O47-Cr24-Zn12	83	0	33	1	34
O48-Cr24-Zn12	84	0	38	0	38
total	--	2810	5682	29793	38285

Supplementary Table 8 | Benchmark of NN calculations for ZnCrO systems against DFT results.

Listed data include the compositions, total atom number per cell (N_{atom}), DFT energy, NN energy and energy differences between DFT energy and NN energy (ΔE , meV/atom).

composition	N_{atom}	E_{DFT} (eV)	E_{NN} (eV)	ΔE (meV/atom)
O6Cr4	10	-78.542	-78.429	-11.340
O6Cr1Zn5	12	-59.509	-59.467	-3.535
O6Cr1Zn5	12	-59.526	-59.542	1.297
O6Cr2Zn4	12	-66.734	-66.795	5.125
O6Cr2Zn4	12	-66.738	-66.787	4.067
O6Cr2Zn4	12	-66.753	-66.719	-2.863
O6Cr3Zn3	12	-72.928	-72.856	-5.997
O6Cr3Zn3	12	-72.977	-72.830	-12.245
O6Cr3Zn3	12	-73.764	-73.763	-0.083
O6Cr4Zn2	12	-78.980	-79.044	5.391
O6Cr4Zn2	12	-78.987	-79.061	6.176
O6Cr4Zn2	12	-80.687	-80.711	1.982
O6Cr5Zn1	12	-86.392	-86.452	4.991
O6Cr5Zn1	12	-86.396	-86.396	0.029
O6Cr5Zn1	12	-86.397	-86.394	-0.285
O8Cr4	12	-86.387	-86.231	-13.005
O8Cr4	12	-88.942	-88.894	-3.998
O7Cr2Zn4	13	-74.166	-74.028	-10.664
O7Cr2Zn4	13	-74.210	-74.077	-10.224
O7Cr3Zn3	13	-80.991	-80.739	-19.440
O7Cr3Zn3	13	-81.039	-80.916	-9.458
O7Cr3Zn3	13	-81.339	-81.081	-19.851
O7Cr4Zn2	13	-87.897	-87.779	-9.058
O7Cr4Zn2	13	-88.309	-88.285	-1.829
O7Cr4Zn2	13	-88.463	-88.370	-7.158
O7Cr6	13	-101.194	-101.082	-8.630
O7Cr6	13	-101.195	-101.077	-9.059
O7Cr6	13	-101.515	-101.178	-25.905
O8Cr3Zn2	13	-83.764	-83.718	-3.549
O8Cr3Zn2	13	-83.883	-83.822	-4.726
O8Cr3Zn2	13	-84.092	-84.065	-2.148
O8Cr4Zn1	13	-92.263	-92.310	3.571
O8Cr4Zn1	13	-92.282	-92.137	-11.154
O8Cr4Zn1	13	-92.321	-92.241	-6.188
O8Cr1Zn5	14	-68.802	-68.782	-1.383

O8Cr1Zn5	14	-68.819	-68.802	-1.223
O8Cr1Zn5	14	-68.911	-69.022	7.925
O8Cr2Zn4	14	-79.328	-79.182	-10.454
O8Cr2Zn4	14	-79.458	-79.153	-21.835
O8Cr3Zn3	14	-88.259	-88.271	0.800
O8Cr3Zn3	14	-88.276	-88.285	0.696
O8Cr3Zn3	14	-88.865	-88.904	2.783
O8Cr4Zn2	14	-96.563	-96.530	-2.326
O8Cr4Zn2	14	-96.955	-96.905	-3.575
O8Cr4Zn2	14	-98.049	-98.049	0.009
O8Cr6	14	-110.235	-110.229	-0.438
O8Cr6	14	-110.268	-110.267	-0.053
O8Cr6	14	-110.452	-110.387	-4.652
O8Zn8	16	-71.258	-71.275	1.111
O8Zn8	16	-71.318	-71.290	-1.707
O8Zn8	16	-71.381	-71.339	-2.596
O15Cr8Zn4	27	-186.335	-186.054	-10.408
O18Cr6Zn6	30	-185.808	-185.656	-5.049
O18Zn2Cr10	30	-219.845	-219.964	3.954
O18Zn2Cr10	30	-219.851	-220.116	8.852
O18Zn4Cr8	30	-202.250	-201.987	-8.774
O18Zn4Cr8	30	-202.265	-201.981	-9.454
O32Cr16Zn1	49	-352.682	-352.425	-5.243
O32Cr16Zn1	49	-355.141	-354.900	-4.915
O32Cr16Zn2	50	-361.449	-361.407	-0.841
O32Cr16Zn2	50	-361.507	-361.211	-5.915
O32Cr16Zn2	50	-362.272	-362.292	0.388
O32Cr16Zn3	51	-367.163	-366.698	-9.110
O32Cr16Zn3	51	-367.315	-366.645	-13.144
O32Cr16Zn4	52	-369.765	-369.581	-3.530
O32Cr16Zn4	52	-369.960	-369.535	-8.180
O32Cr16Zn4	52	-371.105	-371.842	14.176
O32Cr16Zn5	53	-375.053	-375.189	2.583
O32Cr16Zn5	53	-375.529	-375.266	-4.965
O32Cr16Zn5	53	-375.537	-375.307	-4.348
O32Cr16Zn6	54	-380.886	-380.906	0.364
O32Cr16Zn6	54	-381.092	-380.901	-3.524
O32Cr16Zn6	54	-381.099	-380.911	-3.469
O32Cr16Zn7	55	-385.716	-385.983	4.858
O32Cr16Zn7	55	-385.717	-385.906	3.434
O32Cr16Zn7	55	-386.609	-386.747	2.515
O32Cr16Zn8	56	-390.011	-389.812	-3.562
O32Cr16Zn8	56	-390.152	-389.870	-5.047
O32Cr16Zn8	56	-392.219	-392.209	-0.171

* Mean error between DFT energy and NN energy is 6.88 meV/atom.

Supplementary Table 9 | The sensitive analysis of U values. The lattice parameters of CrO₂ and ZnCr₂O₄, the formation energies of ZnCr₂O₄ and Zn₃Cr₃O₈ with respect to ZnO, CrO₂ and O₂, and the band gap of ZnCr₂O₄ with different U value in PBE+U calculations are calculated and compared.

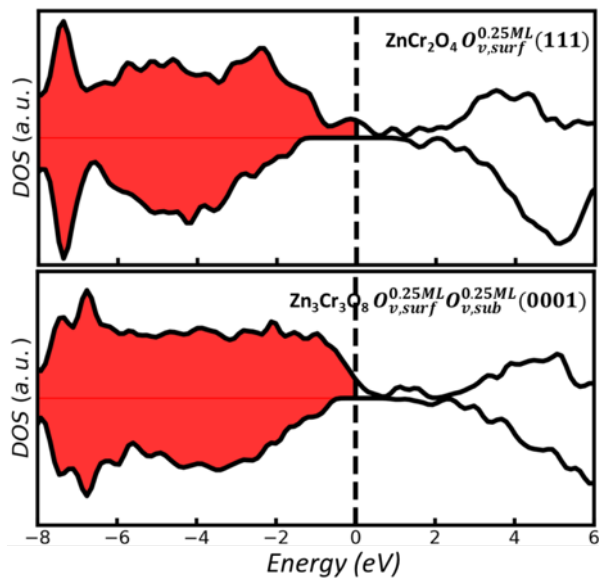
U value	Lattice Parameters		Formation Energy		Band gap ZnCr ₂ O ₄
	CrO ₂ (a/c)	ZnCr ₂ O ₄ (a)	ZnCr ₂ O ₄	Zn ₃ Cr ₃ O ₈	
1	4.410/2.920	8.356	0.170	0.114	1.56
2	4.418/2.933	8.374	0.027	0.036	1.95
3	4.425/2.947	8.389	-0.107	-0.030	2.43
3.3 (This work)	4.437/2.948	8.395	-0.122	-0.044	2.44
4	4.439/2.961	8.403	-0.227	-0.095	2.67
5	4.455/2.976	8.418	-0.340	-0.168	2.92
Exp.	4.419/2.912 ^a	8.327 ^b	-	-	2.90 ~ 3.25 ^c

^a Wang Y.K. et al., *J. Magn. Magn. Mater.*, **2004**, 282, 139.

^b Bertoldi M. et al., *J. Chem. Soc., Faraday Trans.*, **1988**, 84, 1405.

^c Dumitru R. et al., *Catalysts*, **2018**, 8, 210.

For the U values, we have analysed the sensitivity of the Cr oxidation state on U value by benchmarking with experimental data. The results are listed in Supplementary Table 9. As shown, we found the U values in between 3-4 eV provide generally similar results for Cr at different oxidation states. Too large U will destroy the structure prediction, while too low U generally gives wrong band gap and energetics. In particular, only for U value larger than 3 eV, the ZnCr₂O₄ phase, known in experiment as the most stable structure for ZnCrO, is predicted to be the stable structure with respect to the individual component (ZnO, CrO₂ and O₂).



Supplementary Figure 9 | The Density of states (DOS) of ZnCr_2O_4 $O_{v,surf}^{0.25ML}$ (111) and $\text{Zn}_3\text{Cr}_3\text{O}_8$ $O_{v,surf}^{0.25ML}O_{v,sub}^{0.25ML}$ (0001) surfaces calculated by HSE06 functional.

We have confirmed the correctness of DOS results from DFT+U calculations by using hybrid HSE06 functional calculations, as shown in Supplementary Figure 9. The HSE06 DOS also shows the metallic properties for these two O-defective surfaces, which is the same as the DFT+U results in Figure 4b and c.

Supplementary References

1. Song, H. *et al.* Spinel-structured ZnCr_2O_4 with excess Zn is the active $\text{ZnO}/\text{Cr}_2\text{O}_3$ catalyst for high-temperature methanol synthesis. *ACS Catal.* **7**, 7610-7622 (2017).
2. Kulkarni, A. J., Zhou, M., Sarasamak, K. & Limpijumnong, S. Novel phase transformation in ZnO nanowires under tensile loading. *Phys. Rev. Lett.* **97**, 105502 (2006).
3. Giamello, E., Fubini, B., Bertoldi, M. & Vaccari, A. Structure and reactivity of zinc-chromium mixed oxides. Part 3.-The surface interaction with carbon monoxide. *J. Chem. Soc., Faraday Trans.* **85**, 237-249 (1989).